Autonomous Satellite Navigation by Stellar Refraction

Robert Gounley,* Robert White,† and Eliezer Gai‡
The Charles Stark Draper Laboratory, Inc., Cambridge, Massachusetts

This paper describes the error analysis of an autonomous navigator using refraction measurements of starlight passing through the upper atmosphere. The analysis is based on a discrete linear Kalman filter. The filter generated steady-state values of navigator performance for a variety of test cases. Results of these simulations show that in low-Earth orbit position-error standard deviations of less than 0.100 km may be obtained using only 40 star sightings per orbit.

Introduction

An autonomous navigation system is a satellite subsystem designed to estimate the spacecraft's current position and velocity without assistance from ground tracking. Such systems can detect deviations from a desired trajectory and thus enable satellites to initiate their own orbital corrections. The real-time acquisition of satellite position may also assist the performance of other mission functions. With these capabilities incorporated within a satellite its users can benefit from lower maintenance costs and assured mission continuity should terrestrial tracking or communication be interrupted for extended periods.[1,2]

Many autonomous navigation schemes, drawing from a wide range of methodologies, have been proposed and a few implemented. One important class of navigators uses angular measurements between the sun or fixed stars and the limb of the Earth to update satellite position. Although, in concept, systems of this type are simple, their accuracy and utility have been limited by the difficulty of sensing the Earth's horizon precisely. The horizon, viewed from orbit, appears as diffuse atmospheric bands gradually blending into the darkness of space; the edge of the Earth's surface is completely obscured. Consequently, limb-sensing navigators are presented with an inherently ill-defined target with which to chart the satellite's course.[3]

It is proposed that an autonomous navigation system use measurements of refracted starlight to sense the depth of the interposing atmosphere. The problem of directly detecting the Earth's horizon is circumvented by using stellar observations and knowledge of the optical properties of the atmosphere to infer the location of the Earth's surface. The method is simple and, because it utilizes multiple-star observations, provides inputs for autonomous attitude determination. The passage of starlight through the Earth's atmosphere bends the rays inward (see Fig. 1). Viewed from orbit, a setting star's image persists along the Earth's limb well after its true position has passed below the horizon. This refraction is greatest near the Earth's surface and grows progressively weaker at higher altitudes. The starlight refraction angle, R, may be expressed in terms of the tangent height, h_t, of the refracted ray. To a much smaller extent the refraction angle also depends upon the local Earth latitude, season, and time of day; the details of the functional relationships do not affect the error analysis to follow. Recent test data show that the refraction angle can be accurately predicted over much of the Earth using existing atmospheric models.[4]

If we assume the atmosphere to be spherically symmetric, then the refraction angle, R, depends only upon the tangent altitude, h_t. The locus of starlight observed to be refracted by a specific amount forms a cone in space whose rim encircles the Earth at altitude h_t and whose axis is along the star's direction vector u_s (see Figs. 2 and 3). For every star there is an infinite set of refraction cones corresponding to an infinite set of tangent altitudes.

Given perfect measurements, the observation of a star's refraction indicates that the satellite's position is somewhere on the surface of the cone corresponding to the measured refraction angle. To indicate the vector to the satellite's most probable position, the update direction, u_{up}, is oriented normal to the cone's surface as taken from the satellite's estimated position before measurement. Insofar as the refraction angle is extremely small ($\approx$150 arc-sec at 25 km tangent altitude), the cone is essentially a cylinder and u_{up} may be conveniently expressed as the normal to the cylindrical surface as follows:

$$u_{up} = \text{unit}\,[(u_s \times r) \times u_s] \tag{1}$$

where u_s is the unit vector toward a star and r the satellite position at time of measurement. Optimal estimation methods are used to define satellite position based upon measurements made throughout the orbit.

The proposed navigator tracks stars appearing close to the Earth's horizon. In time it observes and identifies a potential grazing star, one whose light will pass through the upper atmosphere. The navigator then locates an unrefracted star for reference and follows the grazing star's shift in apparent position (see Fig. 4). Applying the measured refraction angle to an atmospheric model, the tangent altitude of the incident starlight ray is estimated. Using this measurement, the navigator updates the position and velocity and prepares for the next measurement. If desired, the two star sightings also may be used to estimate current spacecraft attitude.

This paper describes an error analysis of the proposed navigator whereby its potential steady-state positional accuracy is estimated. Several parameters were varied to determine the sensitivity of navigator performance to each of them.

Submitted April 5, 1983; revision received July 20, 1983; presented as Paper 83-2211 at the AIAA Guidance and Control Conference, Gatlinburg, Tenn., Aug. 15-17, 1983.

*Draper Fellow; currently Staff Engineer, Jet Propulsion Laboratory, Pasadena, Calif.

†Section Chief, Systems Engineering Division.

‡Section Chief, Integrated Systems and Control Division. Member AIAA.

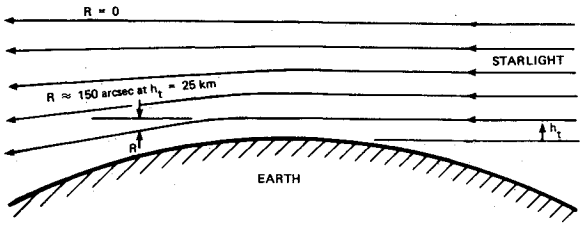

Fig. 1 Variation of atmospheric refraction, R, with altitude, h_t.

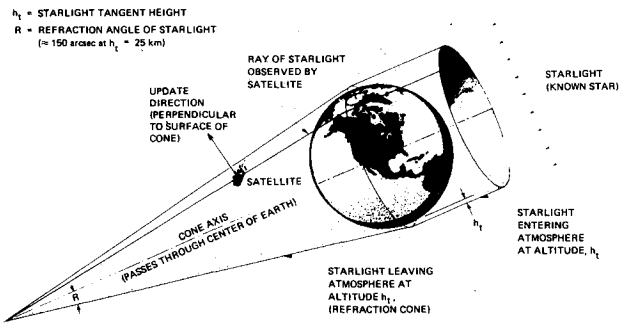

Fig. 2 Satellite navigation using refraction measurements of starlight.

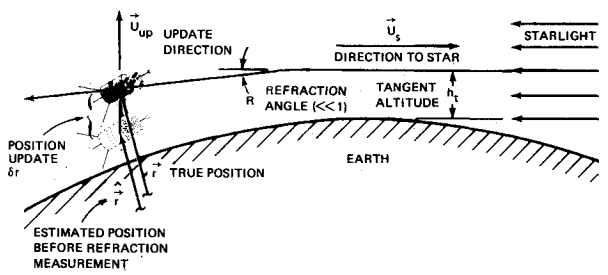

Fig. 3 Geometry of update direction.

Error Analysis

Theory

The analysis of navigation errors for this scheme was performed based on linear covariance analysis, a well-established methodology for evaluating navigation systems.[5] The state variables are linearized about the predetermined nominal trajectory and their covariances calculated at discrete intervals throughout the orbit; the actual trajectory is not estimated.

Let $r(t)$ and $v(t)$ represent the nominal position and velocity vectors at time t. We define $x(t)$ as a seven-dimensional state vector given by

$$x^T = (r^T, v^T, b) \tag{2}$$

where b is the scalar bias in measurements of the tangent height.

The error covariance matrix is defined as

$$P_x(t) = E\{\delta x(t)\ \delta x^T(t)\} \tag{3}$$

where $\delta x(t)$ is the deviation of the state vector from the nominal trajectory.

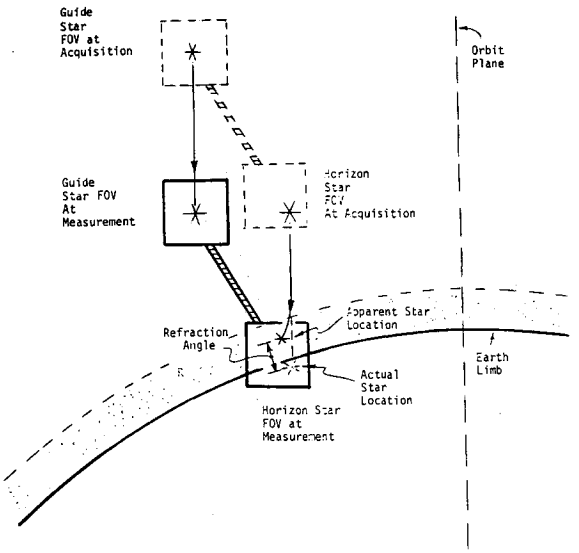

Fig. 4 Navigator fields of view at time of acquisition and time of refraction angle measurement.

The covariance matrix will be propagated from time t_0 to time t using the 7×7 transition matrix $\Phi(t,t_0)$

$$P_x(t) = \Phi(t,t_0)\ P_x(t_0)\ \Phi^T(t,t_0) \tag{4}$$

The elements of the transition matrix for a Keplerian orbit can be derived in closed form as shown in Ref. 6. Those acceleration effects not included in the transition matrix such as gravitational harmonic coefficients, solar pressure, and atmospheric drag are lumped together and modeled as an additive uncorrelated process noise with zero mean and covariance Q. To keep the covariance matrix $P_x(t)$ from diverging, measurements are used for updates. It is assumed that these scalar measurements $z(t_i)$ are functions of the position and velocity vectors, i.e.,

$$z(t_i) = h(r(t), v(t), b(t)) \tag{5}$$

By linearizing the above relationship, the measurement is related to the state vector x

$$z(t_i) = Hx + w \tag{6}$$

where w is the measurement random error with zero mean and variance σ_z^2.

Updates to the covariance matrix are performed using H and σ_z^2 as defined above and

$$P_x(t_i^+) = [I - K(t_i)H(t_i)]P_x(t_i^-) \tag{7}$$

where $(+)$ indicates conditions after the update and $(-)$ indicates conditions before the update. The gain vector $K(t_i)$ is given by

$$K(t_i) = P_x(t_i^-)H^T(t_i)\,[H(t_i)P_x(t_i^-)H^T(t_i) + \sigma_z^2]^{-1} \tag{8}$$

To derive the measurement matrix H the measurement process must be linearized. Relating the refraction angle to the linearized measurement update is rather cumbersome. However, since there is a nonlinear relationship between the refraction angle and the tangent altitude which can be linearized for small perturbations, the tangent altitude may be used as the effective measurement in the update equation.

Assuming a spherical Earth, the geometry of Fig. 3 gives

$$h_t = r^T u_{up} - r_e + |r^T u_s| tgR \tag{9}$$

where r_e is the Earth radius and R is the refraction angle.

For the purpose of computing the measurement matrix H, the last term in Eq. (9) can be neglected. Since u_{up} is not a function of v, the measurement h_t is a function of position only and H is given by

$$H = \frac{\partial h_t}{\partial x} = \left[\frac{\partial h_t}{\partial r}, \quad 0_{1\times 3}, \quad 1\right] \tag{10}$$

or

$$H = \left[u_{up}^T, \quad 0_{1\times 3}, \quad 1\right] \tag{11}$$

because it can be shown[7] that

$$r^T \frac{\partial u_{up}}{\partial r} = 0 \tag{12}$$

Implementation

The results of the error analysis are visualized more readily when viewed in terms of the satellite-centered coordinate system TNR (tangential, normal, radial). The coordinates for this system are:

u_R = directed toward the Earth along the position vector

u_N = normal to the orbital plane and pointing in the opposite direction to the orbit's angular momentum vector

u_T = orthogonal to u_R and u_N and directed in same sense as the satellite's velocity vector

Figure 5 shows u_{up} and u_s in TNR coordinates. The azimuth angle ϕ specifies a position rotation about the u_R axis. The horizontal elevation angle θ specifies the angle between the star direction and downward u_R when the star's light grazes the atmosphere (see Fig. 6).

The error analysis presumes that the navigator contains a simple dynamic model of two-body orbital motion perturbed by the gravitational harmonic coefficient J_2. Therefore, the amount of process error noise used in the analysis is based upon the magnitude of all other sources of orbital perturbation—these include higher-order gravitational harmonics, atmospheric drag, and solar pressure.

The selection of stars for navigation are made on the basis of their brightnesses and azimuths. The azimuth span specifies a wedge of the sky to be searched by the navigator for grazing stars (see Fig. 7). Setting stars (azimuths between 90 and 270 deg) are preferred because rising stars are difficult to locate quickly amid atmospheric haze. Furthermore, stars grazing near ±90-deg azimuth may also be undesirable since they will take longer to undergo refraction than those close to the orbital plane. For most of the cases studied the azimuth span was kept between 135 and 225 deg.

The simulations performed create observations of grazing stars at random intervals along the assumed orbit. To approximate what an actual navigator would observe, random sighting times and azimuths are generated in a manner consistent with a uniform distribution of stars throughout the sky.

The uncertainty associated with estimating the tangent altitude is a function of both the refraction measurement error and the atmospheric density uncertainty. The approximate relationship is given as follows:

$$dh_t = H\frac{d\rho_0}{\rho_0} - H\frac{dR}{R} - D\,dR \tag{13}$$

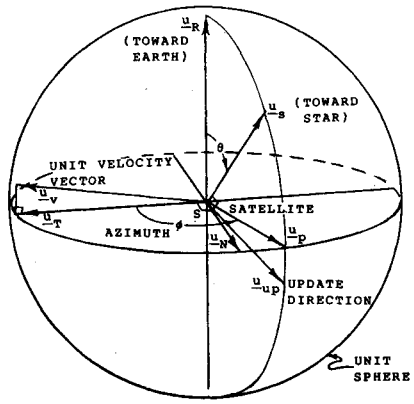

Fig. 5 Direction of position update in satellite-centered coordinates.

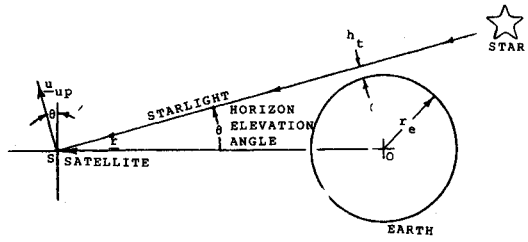

Fig. 6 Definition of horizon elevation angle.

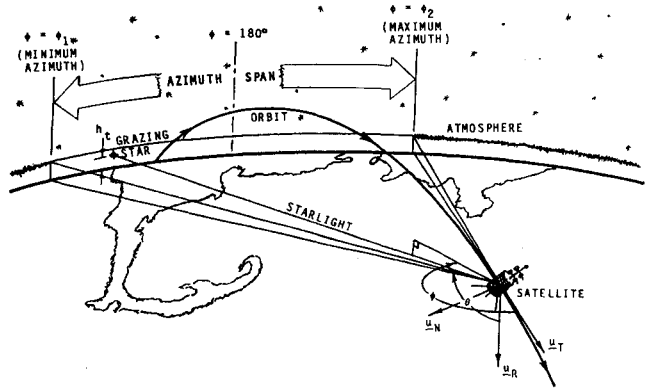

Fig. 7 Description of azimuth span.

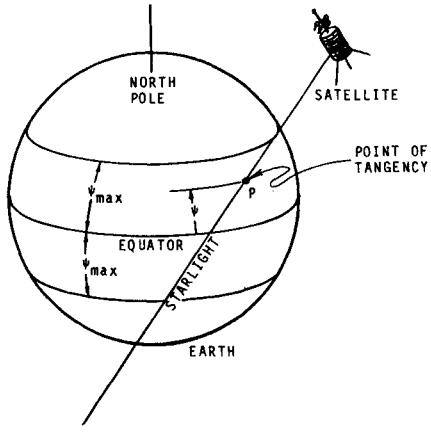

Fig. 8 Measurement restrictions due to grazing latitude.

where dh_t is the tangent altitude error caused by a density error, $d\rho_0$, and refraction error, dR; H is the density scale height (~6.4 km at 25 km altitude); and D is the satellite distance from the base of the refraction cone. Equation (13) indicates that the tangent altitude error is proportional to the percentage error in density and refraction and to the refraction error times the distance to the horizon (or cone base). Since fairly high refraction measurement accuracies can now be achieved with star sensors, it is felt that the potential accuracy of this navigation concept is limited primarily by the uncertainty in atmospheric density. Stratospheric observations with meteorological rockets and balloons indicate a density uncertainty at 25 km altitude of about 1.3% in the tropical region.[8,9] For the summer hemisphere the indicated density uncertainty may increase by a factor of two or three when going from the equator to the pole. However, the winter hemisphere, especially in the north, may experience local variations as high as 10%. It should be noted that most of the above data is based on temperature measurements which have been combined with pressure estimates to obtain density estimates. The errors in the density estimates for a given observation have generally been no better than 1 or 2%. Consequently, further reductions in the density uncertainties are likely through the use of more accurate measurements and improved density modeling. This could be achieved with accurate satellite observations of atmospheric refraction since such observations in combination with satellite ephemeris data can be used to estimate density. Experiments of this type have already been conducted by one of the authors with refraction data from the Orbiting Astronomical Observatory (OAO-3) and the High Energy Astronomy Observatory (HEAO-2).

In the present study, the baseline value adopted for the measurement noise in tangent height was 70 m. According to Eq. (13) this corresponds to an equivalent density error of 1.1% or an equivalent refraction error of 1.2 arc-sec (i.e., assuming a refraction of 148 arc-sec for a tangent altitude of 25 km and a satellite altitude of 920 km). Since sub-arc-sec accuracies can now be achieved in refraction measurements, the tangent height measurement accuracy primarily will be limited by the density uncertainty. If there were no error in the refraction measurement, it is seen that the 70 m would be fairly representative of observations in the tropical region. This would also be the case for some other regions of apparent stability in the world. However, if there were no observation restrictions, then a *larger* tangent height error should be used, and the sensitivity results in this paper provide some indication of what that performance would be.

To account for regional mismodelings, a measurement bias b was included in the state vector x. It is important to note that a more elaborate set of systematic and bias type errors could have been included in the state vector. However, for the purposes of this study, only a bias error was assumed to be present outside an equatorial band defined by the latitude ψ_{max} in Fig. 8. Inside this band, the measurement was assumed to be unbiased. This was reflected in the measurement matrix H by assigning

$$H = [\boldsymbol{u}_{up}^T, \quad 0_{1\times 3}, \quad 0]_{1\times 7} \tag{14}$$

for star sightings over equatorial regions and

$$H = [\boldsymbol{u}_{up}^T, \quad 0_{1\times 3}, \quad 1]_{1\times 7} \tag{15}$$

otherwise.

Results

Baseline Parameters

The parameters listed in Table 1 were used to establish baseline navigator performance.

Table 1 Baseline parameters

Orbit	
Semimajor axis, a	7293.27 km (497 n.mi. altitude)
Eccentricity, e	1.809×10^{-5}
Inclination, i	65.00 deg
Longitude of ascending mode, Ω	0.00 deg
Measurements	
Tangent altitude, h_t	25 km
No. of star sightings per orbit, N	40
Maximum grazing latitude without measurement bias, ψ_g	30.00 deg
Azimuth span	$135 \text{ deg} < \phi \leq 225 \text{ deg}$
Filter	
Measurement variance, σ_z^2	$(0.070 \text{ km})^2$
Time step for propagation, Δt	30 s
Process noise covariance matrix (excluding the effects of the gravitational harmonic coefficient, J_2):	

$$Q_i = \begin{bmatrix} 0_{3\times 3} & 0_{3\times 3} & \\ 0_{3\times 3} & qI_{3\times 3} & 0 \\ & 0_{1\times 6} & 0 \end{bmatrix}$$

where $q = 6.0 \times 10^{-14} \text{ km}^2/\text{s}^2$

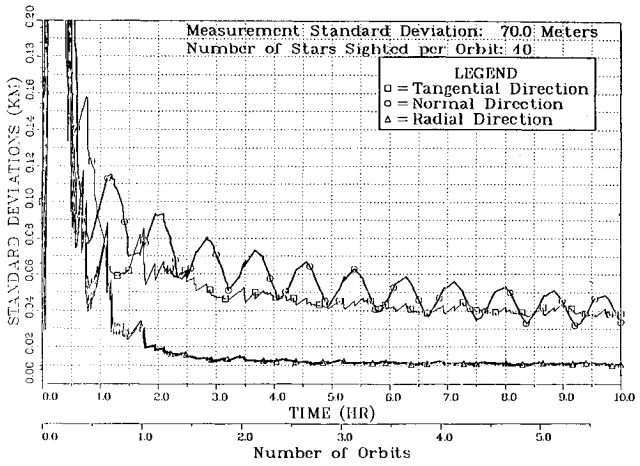

Fig. 9 Time history of navigator position error standard deviations.

Baseline Results

The baseline time history for position error standard deviations (tangential, normal, and radial) is shown in Fig. 9. During the first few orbital periods the navigator filter develops very large position error transients as it tries to sense the orbital motion from the measurements. This time history is typical for the simulations performed.

As starting transients die out (typically after a few orbits) the navigator's position error standard deviations tend to oscillate about constant values; this steady-state behavior is very nearly achieved after only two periods of rotation. Since the three components of navigator error oscillate asynchronously, it would be misleading to quantify the navigator's steady-state accuracy based upon the filter results at a specific time. A more consistent and representative set of values is obtained by performing a linear least-squares fit of the data

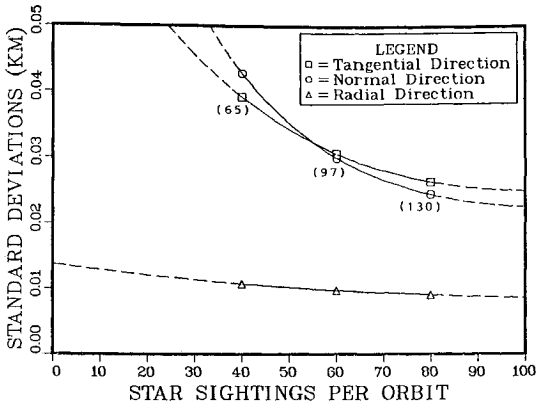

Fig. 10 Sensitivity of navigator to number of star sightings (low-Earth orbit).

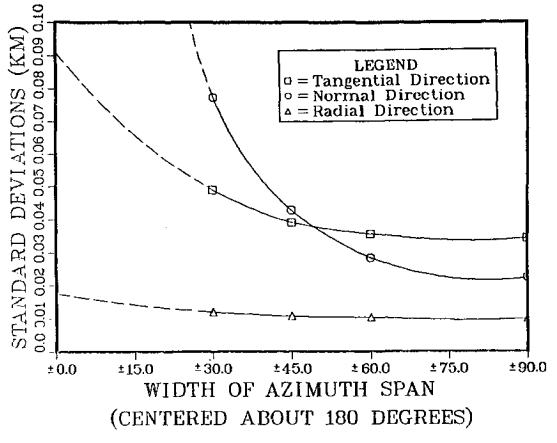

Fig. 11 Sensitivity of navigator to width of azimuth span (low-Earth orbit).

over the last period and extrapolating the resulting line to the final time. For the baseline case, the averaged estimates of the position error standard deviations in satellite-centered inertial coordinates are: tangential direction, 0.039 km; normal direction, 0.043 km; and radial direction, 0.011 km.

Sensitivity Studies

Figure 10 shows the effect of increasing the number of star sightings per orbit. Tangential and normal components of error remain the same, while the radial component is small. The trend indicates that relatively little improvement may be expected by increasing the number of star sightings beyond the baseline value of 40.

Increasing the size of the azimuth span widens the sector of the sky surveyed and thus makes more stars available for navigation. The added stars have directions more nearly perpendicular to the orbital plane; sighting these stars enhances the navigator's position estimate in the normal direction. These improvements must be weighed against the potential implementation problems of observing stars far out of the orbital plane.

For the simulations shown in Fig. 11, the width of the azimuth span was varied about a 180-deg centerline. Note that the normal component is improved greatly as the azimuth span is widened. The tangential component is improved less substantially while the radial component is virtually unaffected.

Increasing the size of the azimuth span widens the sector of the sky surveyed and thus makes more stars available for navigation. The added stars have directions more nearly perpendicular to the orbital plane; sighting these stars enhances

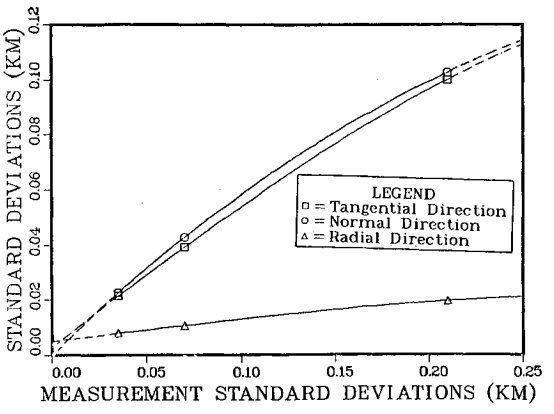

Fig. 12 Sensitivity of navigator to measurement uncertainties (low-Earth orbit).

the navigator's position estimate in the normal direction. These improvements must be weighed against the potential implementation problems of observing stars far out of the orbital plane.

For the simulations shown in Fig. 11, the width of the azimuth span was varied about a 180-deg centerline. Note that the normal component is improved greatly as the azimuth span is widened. The tangential component is improved less substantially while the radial compent is virtually unaffected.

The low position error standard deviations predicted by the filter are due, in large part, to the small measurement error variance used (0.0049 km^2). While it is felt that state-of-the-art sensor technology and atmospheric modeling can deliver this magnitude of measurement accuracy, it is instructive to examine the effects of varying the tangent height error variance on the navigator's performance. The results of this sensitivity study, shown in Fig. 12, indicate that navigator performance is not severely affected by less accurate observations. Measurements containing three times the baseline error standard deviation produce much less than a three-fold increase in the navigator's position error standard deviations.

Conclusions

For the input parameters considered, covariance studies indicate that the proposed autonomous navigator can estimate position to standard deviations of less than 0.100 km. This high accuracy is achievable using only a small number of star sightings per orbit. The convergence to steady-state performance is rapid—typically a few orbits.

Sensitivity studies show that increasing the number of sightings per orbit beyond the baseline value of 40 yields only a modest improvement in navigator accuracy. Widening the azimuth span in which stars are sighted also improves performance, especially in the normal direction.

Acknowledgments

The authors would like to thank Milton B. Adams, Steven R. Hall, and James V. Harrison for their suggestions.

References

[1] Paulson, D. C., "Autonomous Satellite Navigation from Strapdown Landmark Measurements," *Proceedings of the 3rd Symposium on Nonlinear Estimation Theory*, San Diego, Calif., Sept. 1972, pp. 167-182.

[2]Lowrie, J. W., "Autonomous Navigation Systems Technology Assessment," AIAA Paper 79-0056, Jan. 1979.

[3]Fang, B. T., "Satellite-to-Satellite Tracking Orbit Determination," *Journal of Guidance and Control*, Vol. 2, Jan.-Feb. 1979, pp. 57-64.

[4]Barnes, F., "Earth Horizon Sensing by Stellar Refraction Measurement," The Charles Stark Draper Laboratory, Inc., Cambridge, Mass., Intralab Memo. AGS-25-75, Oct. 16, 1975.

[5]Gelb, A., ed., *Applied Optimal Estimation*, MIT Press, Cambridge, Mass., 1974.

[6]Goodyear, W. H., "Completely General Closed-Form Solution for Coordinates and Partial Derivatives of the Two-Body Problem," *Astronomical Journal*, Vol. 70, No. 3, April 1965, pp. 189-192.

[7]Gounley, R. B., "Error Analysis of an Autonomous Navigation System Utilizing Refraction Measurements of Starlight," The Charles Stark Draper Laboratory Inc., Cambridge, Mass., Rept. CSDL-T-790, Aug. 1982.

[8]Cole, A. E. and Kantor, A. J., "Air Force Reference Atmospheres," Air Force Geophysics Laboratory, Rept. AFGL-TR-78-0051, Feb. 28, 1978.

[9]Cole, A. E., Kantor, A. J., and Philbrick, C. R., "Kwajalein Reference Atmospheres, 1978," Air Force Geophysics Laboratory, Hanscom AFB, Doc. AFGL-TR-79-0241, Sept. 24, 1978.